ELSEVIER

Surface and Coatings Technology 82 (1996) 176–186

SURFACE & COATINGS TECHNOLOGY

Rolling contact fatigue behaviour of thermally sprayed rolling elements

R. Ahmed, M. Hadfield

Department of Mechanical Engineering, Brunel University, Uxbridge, Middlesex UB8 3PH, UK

Received 7 August 1995; accepted in final form 30 October 1995

Abstract

An experimental approach with a modified four-ball machine is used to investigate the rolling contact fatigue (RCF) performance and failure mode of thermally sprayed rolling element bearing steel balls. A superdetonation gun (SDG 2040) is used to deposit a tungsten carbide coating (WC–15%Co) on steel substrate balls. This test configuration has been used to simulate traditional steel and ceramic hybrid rolling element ball-bearings. Microhardness of coating and substrate, scanning electron microscopy (SEM) and finite element modelling (FEM) of the contact problem for coated elements are the key tools in the analysis. The results show that coated specimens do not perform well and the failure is through the coating itself and not at the interface. Results from FEM and SEM of failed areas indicate that the failure of coatings is in plain shear at the edge of the contact area. An improvement is required in the coating technique for rolling contact fatigue application. Advanced processes such as high velocity oxy-fuel (HVOF), etc. may provide different results. The mode of failure in the coated specimens is delamination.

Keywords: Thermal spray; Carbide; Finite element modelling; Rolling contact fatigue

1. Introduction

1.1. Background

Thermal spray coatings deposited by techniques such as detonation gun (D-gun), high velocity oxy-fuel (HVOF), arc wire, etc. are extensively used to coat components in the aerospace industry. The advantages offered by these surface modification techniques are helpful in providing improved and reliable performance of components in other sectors of industry, e.g. power generation and the automobile industry [1]. Applications such as clearance control, thermal barrier, wear resistance, etc. are common in the field of thermal spraying. Metal carbide coatings represent a family of coatings which are used to improve the wear resistance of components. Among this family, D-gun-sprayed tungsten carbide coatings are known to display extremely high resistance against sliding wear, hammer wear, abrasion and fretting [2]. It is a well-established fact that the performance of a coating is dependent on application and upon the overall behaviour of the coating and substrate combination. Hence an experimental approach can enable us to investigate the performance and identify the factors which are critical for a specific application. One such application is the rolling element bearing.

In this study a modified four-ball machine simulating a rolling element ball-bearing is used to examine thermally sprayed detonation gun coatings in conventional steel ball-bearing and hybrid ceramic bearing configurations. Coating microhardness, microstructure and finite element modelling (FEM) of coated elements contacting a steel and ceramic ball are also used to investigate the behaviour of these coatings.

Rolling contact fatigue (RCF) is the major phenomenon leading to the failure of rolling element bearing materials. There is an increasing demand for improved life, reliability and load-bearing capacity of bearing materials and future applications call for using them in more hostile environments. Investigation and optimization of techniques used in thermal spraying processes can be helpful in reaching the full potential and improved performance of traditional steel and hybrid ceramic bearings in an economical fashion.

This study addresses the RCF performance of these coatings under various tribological conditions. The purpose of the study is to investigate the failure mode and RCF life of thermal spray coating, since these features can be helpful in tailoring future coatings by providing feedback and thus optimizing their performance for such applications.

1.2. Previous studies

Initial studies by Tobe et al. [3] on the RCF behaviour of plasma-sprayed coatings showed that the delamina-

SSDI 0257-8972(95)02736-X

tion behaviour of some ceramic coatings was preceded by the generation of a blister. They reported that the compressive strength of the coating and the shear strength between coated layer and substrate are the most important factors for RCF performance. Later studies by Keshavan and Kembaiyan [4] showed that the D-gun coating technique can be used to improve the life of thrust bearings in drilling applications. However, a delamination behaviour of WC–Co coatings was observed for radial bearing sleeves. Hadfield et al. [5] reported that the failure mode of some thermal spray coatings in rolling contact applications is delamination. They observed that WC–Co coatings were delaminating from within the coating microstructure while aluminium oxide coatings were delaminating at the interface of coating and substrate.

Although there has been limited research on the RCF application of thermal spray coatings, the results from other coating techniques such as physical vapour deposition (PVD) can be helpful in optimizing the performance. Thom et al. [6] investigated the effect of nitride coatings on 440C stainless steel. They showed that coating thickness is the most important parameter in RCF application. Similarly, Sproul et al. [7] showed that substrate hardness is also critical for RCF performance.

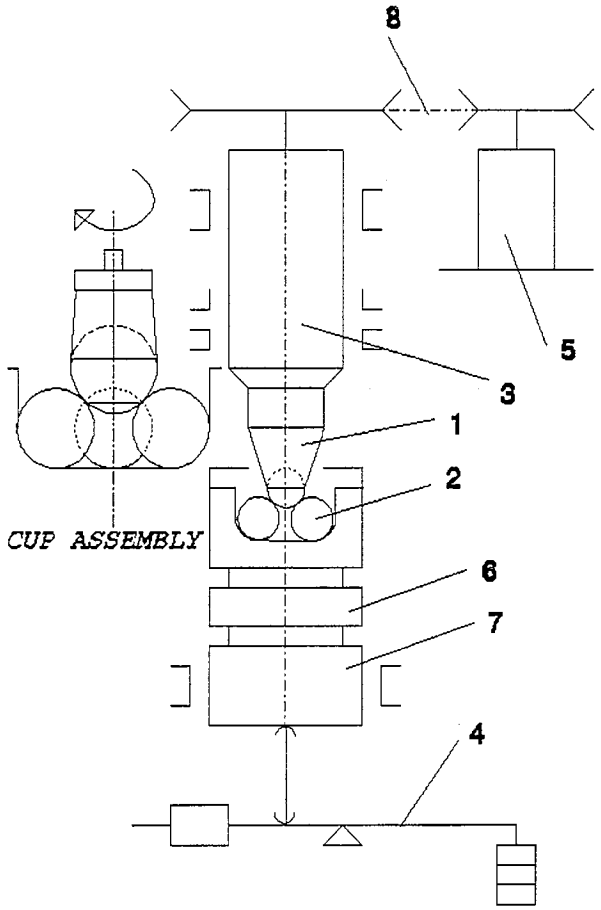

Fig. 1. Schematic diagram of modified four-ball machine: 1, coated ball and collet; 2, lower balls; 3, spindle; 4, loading lever; 5, driving motor; 6, heated plate; 7, loading piston; 8, belt drive.

2. Experimental procedure

2.1. Test configuration

Fig. 1 shows the modified four-ball machine which is used to investigate the rolling contact fatigue performance of coated rolling ball elements. This machine simulates a rolling element bearing configuration and is used as an accelerated method to investigate the rolling contact fatigue resistance of materials under various tribological conditions. The Institute of Petroleum has gathered together various papers [8] which describe test results, ball dynamics and kinematics.

The modified four-ball machine consists of eight major components. A piston under the steel cup is used to load the cup assembly for the generation of required contact stress. The coated ball, which is securely fixed in the spindle through a spring steel collet, contacts the lower planetary balls. The contacting surfaces between the coated ball and the lower planetary balls are immersed in lubricating oil. A thermocouple at the base of this cup is used to monitor the oil bulk temperature during the test.

Spindle speeds may be varied up to 20 000 rev min^{-1} with the help of high or low speed drives. Test times and spindle revolutions are recorded by a timer and tachometer. A vibration sensor, located in the body of the machine near the cup assembly, monitors the vibration in the cup assembly. The machine may be set to stop either at a fixed vibration amplitude or after a certain number of revolutions.

2.2. Coated ball test elements

Tungsten carbide (WC–Co) coatings are well known for their high resistance against wear, corrosion and abrasion. Thermally sprayed WC–Co coatings are produced in industry as standard practice by a variety of methods, e.g. D-gun, HVOF, high velocity air fuel (HVAF), etc. In this study a detonation flame spraying method has been used as the coating process. A super-D-gun (SDG 2040) is used to spray a tungsten carbide coating on the surface of balls of diameter 0.5 in. Only half of the ball is required to be coated for the tests and the material composition of the coating can be summarized as 15% Co, 3% C and 82% WC. The as-sprayed balls have a coating thickness of approximately 100 μm.

The substrate balls are sandblasted prior to the coating process so as to assist strong bonding by mechanical interlocking between the coating and the substrate. Table 1 lists some of the physical properties of the coating. (The Young modulus for WC–Co coatings

Table 1
Physical properties of coating

Physical property	Value
Adhesive strength (MPa)	68.6
Porosity (%)	1.0
Vickers microhardness (HV. 300)	1150
Young modulus (GPa)	524[a]

[a] Average estimated value.

actually changes with the grain size of WC, cobalt content, heat treatment, etc. The value given in Table 1 is an estimate for the coating used.)

2.3. Lower ball contact elements

The selection of lower ball contact elements which serve the purpose of simulating the rolling elements in rolling bearing is based on a traditional steel bearing and a hybrid ceramic bearing design. Thus the two materials used for the lower ball contact elements are bearing steel and silicon nitride ceramic. The steel lower balls are grade 2 (ISO 3290-1975) carbon chromium steel with an average surface roughness of 0.012 μm and Rockwell C hardness of 64 HRC. The silicon nitride is manufactured by the hot isostatic pressing (HIP) method. Ball blanks are ground and polished to a diameter of 0.5 in; standardized procedures are adopted to ensure consistent quality of material and geometry. The average roughness (R_a) of the ceramic ball surface is 0.01 μm and the ball roundness is within standard ball-bearing tolerances.

The cup used to hold these balls serving the purpose of the outer race of rolling contact bearing is designed to simulate type II [8] contact conditions between the cup and the planetary balls. The material used is bearing steel and the hardness of the cup is 60 HRC.

2.4. Sample polishing and thickness control

The lubrication conditions of the contact elements are dependent upon the surface finish of meeting surfaces. Hence it is important to control the surface roughness of coated balls to a reasonable finish. Conventional polishing methods result in a high surface finish of coatings on flat samples. In order to control the surface finish and coating thickness of coated balls, a special technique is designed in which the modified four-ball machine is used to polish the test samples. Fig. 2 shows a schematic diagram of the method, in which a female cup with the impression of half of the ball is held on the piston of the modified four-ball machine. The ball to be polished is held in the spindle and rotated at low speeds, typically 200 rev min^{-1}, and low loads, typically in the region of 4 N, applied to the cup assembly. Initially a

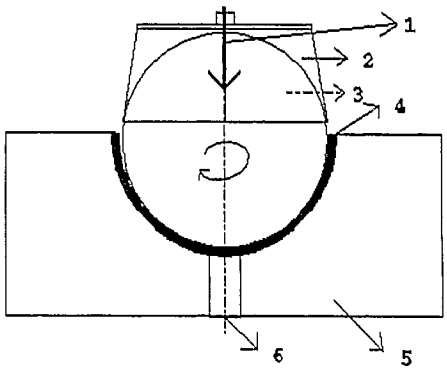

Fig. 2. Schematic diagram of polishing method: 1, applied load; 2, collet; 3, sample for polishing; 4, polishing cloth; 5, cup; 6, hole for debris.

nylon polishing cloth and then a DP-Nap cloth are used with different grades of diamond paste in between the rotating ball and the stationary female cup. The final stage of polishing involves using a diamond slurry and a soft cotton cloth. The technique has been optimized by using different materials for the cup and polishing cloth as well as varying the load and speed during polishing. The use of cotton cloth in the final stage of polishing is important, because a soft cloth deforms well and follows the profile of the cup, whereas a conventional final polishing cloth leaves polishing marks on the surface. A Talysurf with step motor is used to measure the surface roughness of polished samples. The machine is calibrated before the measurements and the average R_a of polished coated balls is measured to be in the region of 0.02 μm. The machine filter used is guassian and the cut-off used is 0.25 mm.

In order to control the thickness of coating, the tip of the ball is ground off and observed under a high magnification microscope. The radii of two emerging concentric circles are used to calculate the coating thickness with the aid of basic trigonometric relations. Fig. 3 represents a typical result in which the coating thickness is measured as 50 μm.

2.5. Microhardness measurements

Leitz miniload 2, Vickers, Knoop and scratch hardness testers are used to measure the microhardness of the coating and substrate at various geometrical locations. The surface exposed after grinding the tip of the cone (for thickness control measurements) is utilized for these measurements. The surface is polished using diamond paste by conventional methods to get a smooth flat surface. Measurements on a typical ball at loads of 100 p and 300 p reveal an average microhardness of 1200 HV for the coating and 600 HV for the substrate. The mean values of the hardness readings are calculated after neglecting the maximum and minimum values. The location of these hardness measurements can be seen in

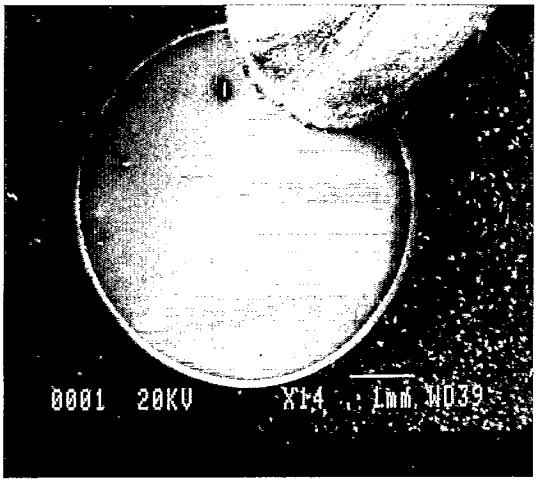

Fig. 3. Coating thickness.

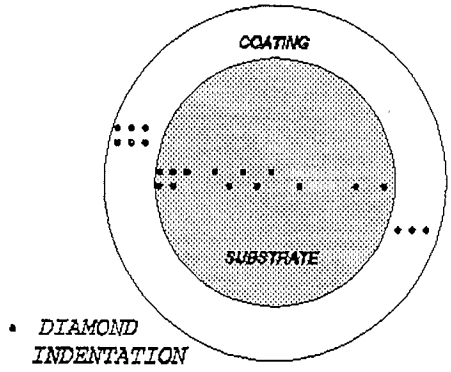

Fig. 4. Location of microhardness measurements.

Fig. 4. The major objective of this analysis is to investigate the variation in hardness of the coating and substrate. The tests revealed that the hardness of the coating varies from 1100 to 1500 HV while that of the substrate varies from 560 to 680 HV.

The variation in the microhardness of the coating is mainly due to the lamellar structure of the coating. Higher hardness values up to 1500 HV are mainly due to the presence of secondary phase particles such as W_2C, etc. This is consistent with the hardness analysis presented by Wira et al. [9]. Results also indicate that the substrate microhardness increases near the interface and is mainly due to the temperature prevailing during the coating process and the residual stresses imposed by sandblasting prior to coating.

2.6. Lubrication conditions

The test lubricant used in this preliminary study is BP Hitec 174, which is a high viscosity paraffin hydrocarbon lubricant with a kinematic viscosity of 200 cSt °C at 40 °C and 40 cSt °C at 100 °C. This lubricant is not commercially available. Exxon 2389, a synthetic lubricant with a kinematic viscosity of 12.5 cSt °C at 40 °C and 3.2 cSt °C at 100 °C, is also used but not in all the test configurations. Tests were conducted at 4000 rev min^{-1} with loads of 160, 400 and 560 N applied to the cup assembly. Fig. 5 shows the elastohydrodynamic lubrication (EHL) calculation results for the two lubricants.

The results are given in terms of contact configuration

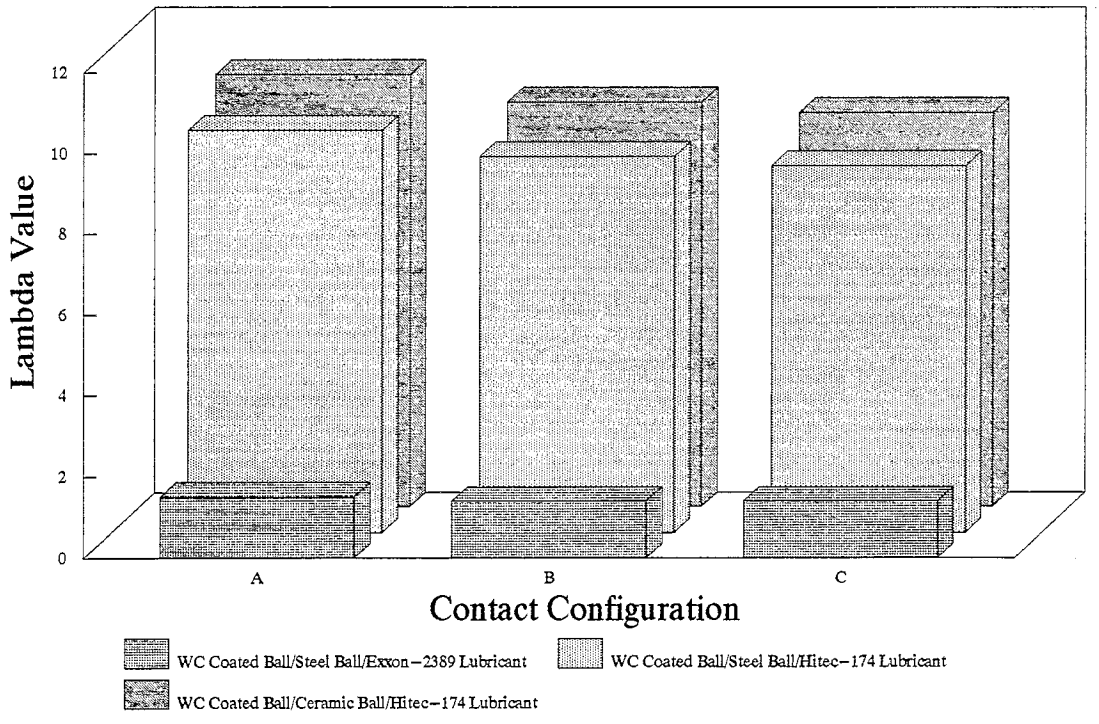

Fig. 5. EHL results: A, 160 N load; B, 400 N load; C, 560 N load.

and ratio of minimum film thickness to average roughness (λ). They have been calculated for minimum film thickness and the details of the method can be found elsewhere [10]. The analysis shows that the tribological conditions for lubrication varied from mixed lubrication for Exxon 2389 lubricant to a fully developed elastohydrodynamic film completely separating the two contacting surfaces for Hitec 174 lubricant.

2.7. Coating microstructure

WC–Co coatings consist of tungsten carbide particles bonded by a cobalt matrix. The WC particles provide hardness whereas the Co matrix provides toughness to the coating microstructure. An investigation of the coating microstructure is carried out to appreciate the homogeneity of the coating. The coated ball is sectioned, mounted, ground and polished using conventional techniques. Fig. 6(a) shows a high magnification scanning electron microscopy (SEM) image of a coating, while Fig. 6(b) shows the corresponding backscattered electron microscopy (BEM) image of the coating. Highly illuminated particles (A) represent high atomic number elements, while tungsten carbide particles (B) are also visible embedded in the cobalt matrix (C). The micrographs show that there are some secondary phase particles and porosity in the coating microstructure.

3. Results and surface observations

3.1. Test results

The test results shown in Fig. 7 illustrate the coating performance under various tribological conditions. The results are given in terms of contact configuration, lubricant and time to failure. These results merely show the performance of the coated elements and are not intended for use as a basis for statistical fatigue life prediction. The test with Exxon 2389 lubricant failed in less than 10 min and so the test results are not presented in Fig. 7.

These test results indicate that the coated balls do not perform well in rolling contact fatigue applications. Another observation which can be appreciated from these results is that the tests with ceramic balls have significantly lower fatigue life than the tests with steel balls. This is mainly because of the higher contact stresses due to the higher hardness and modulus of elasticity of ceramic balls in comparison with steel balls.

3.2. Surface observations

Fig. 8 shows SEM observations of failed tungsten carbide-coated balls against ceramic balls. In these tests the coated balls are tested against ceramic planetary balls at loads of 160 and 400 N applied to the cup assembly. Fig. 8(a) shows the overall failed area for the 160 N test. Fig. 8(b) shows the edge cracks on the failed area. Fig. 8(c) shows the failed area for the 400 N test. The detail of this failure can be appreciated from Fig. 8(d), where cracks are visible not only on the edge of wear track but also within the coating microstructure and the propagation of cracks is also visible. The depth of failure can be seen to be approximately 40 μm. Electron probe microscopy analysis (EPMA) results show tungsten (W) and Co on the failed surfaces, thereby providing that the coatings are not failing at the interface. Some cracks are also observed within the wear track during SEM analysis. The mode of failure in these results is observed to be delamination.

Surface observations for the tests in which coated balls are tested against steel planetary balls are shown in Fig. 9. Fig. 9(a) shows the failed area for a ball tested at 160 N load in Hitec 174 lubricant. The rolling direction in this case is from left to right. Fig. 9(b) shows the

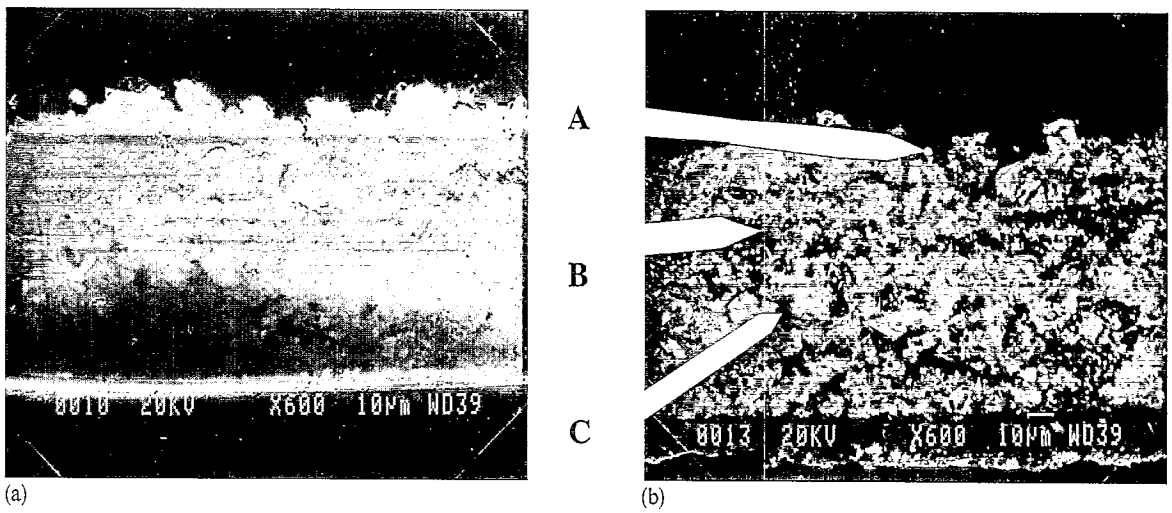

(a) (b)

Fig. 6. Coating microstructure: (a) SEM image; (b) BEM image.

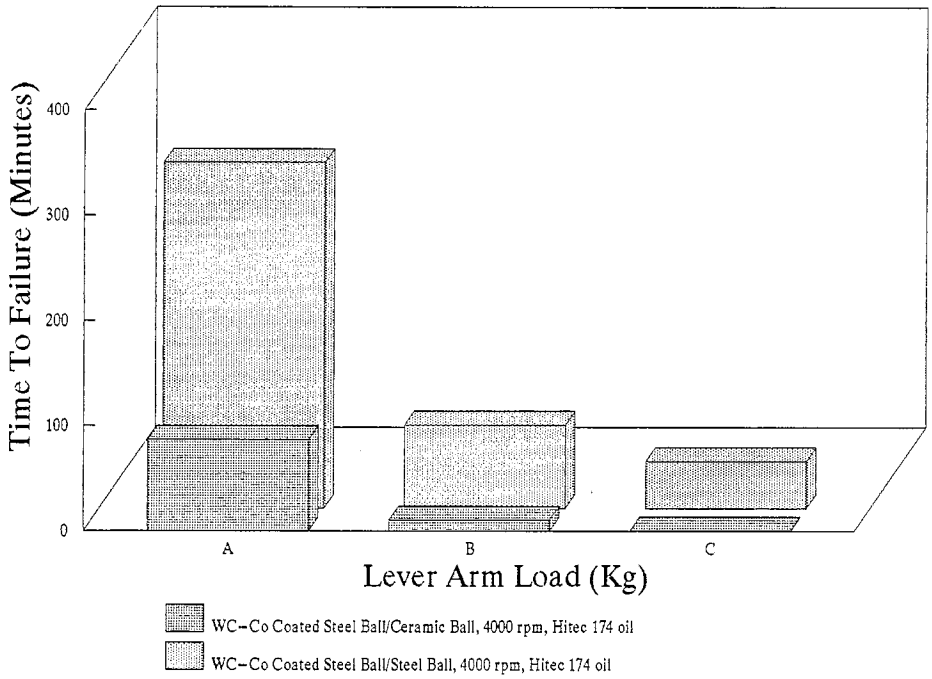

Fig. 7. Rolling contact fatigue test results: A, 160 N load; B, 400 N load; C, 560 N load.

details of cracking on the right-hand-side edge of the failed area. EPMA shows that the failure is within the coating. Fig. 9(c) shows the failed area for a test at 160 N in Exxon 2389 lubricant. The rolling direction is again from left to right. Fig. 9(d) shows the detail of the failed area. The depth of failure in both cases can be estimated as approximately 40 μm. The EPMA results confirm that the failure is through the coating itself and not through the coating–substrate interface.

4. Finite element modelling

A finite element model of a ball of 0.5 in diameter in contact with a coated ball is used to investigate the effects of changes in coating thickness and physical properties such as Young modulus and Poisson ratio on the location and magnitude of stresses generated during contact. It is an axisymmetric model as shown in Fig. 10(a) and consists of 6683 nodes, 2854 isoparametric curvilinear quadrilateral eight-noded elements and 18 isoparametric curvilinear triangular six-noded elements. The axis of symmetry is the X-axis. The accuracy of the model has been verified by comparison with the stress results for uncoated conditions of the model from Hertz theory calculations. The variation in stress values is within 3% of the Hertz stress calculations.

The importance of modelling is evident because of the difficulties involved in calculating the Hertz stresses for coated elements. A finite element model also gives a better understanding of the distribution and location of stresses within the contacting bodies.

Fig. 10(b) presents a summary of the results for various coating configurations and a comparison with the uncoated situation. Two different coating thicknesses, i.e. 60 and 30 μm, are considered. The Young modulus and Poisson ratio are then varied for both thicknesses, keeping all other parameters constant.

Fig. 10(c) shows a schematic diagram of the locations of the various stresses in the coated ball, with the sign conventions as deduced from the FEM results. Owing to the rolling motion of the balls, the magnitude of shear stress in the X–Y plane occurring at location(a) changes from compression to tension and so on. Hence the hysteresis effect causes this value of shear stress to be doubled to what has been shown in the static model in Fig. 10(b). The maximum principal shear, Tresca and von Mises stresses occur at location(b).

Fig. 11(a) presents the stress distribution and magnitude of maximum principal shear stress for a 60 μm coating on a steel substrate contacting a steel ball under 400 N load. Each element shown in Fig. 11 is 15 μm in dimensions. The stress contours for von Mises and Tresca stresses are exactly the same as for maximum principal shear stress, but the magnitude of stress values is different, as can be appreciated from Fig. 10(b). The result of shear stress in the X–Y plane is shown in Fig. 11(b) for the same configuration. The magnitude and location of these stress contours indicate that the maximum principal shear, von Mises and Tresca stresses occur at the interface, whereas the maximum shear stress in the X–Y plane is located at a depth of approximately 40 μm. A stress concentration is also visible at this location.

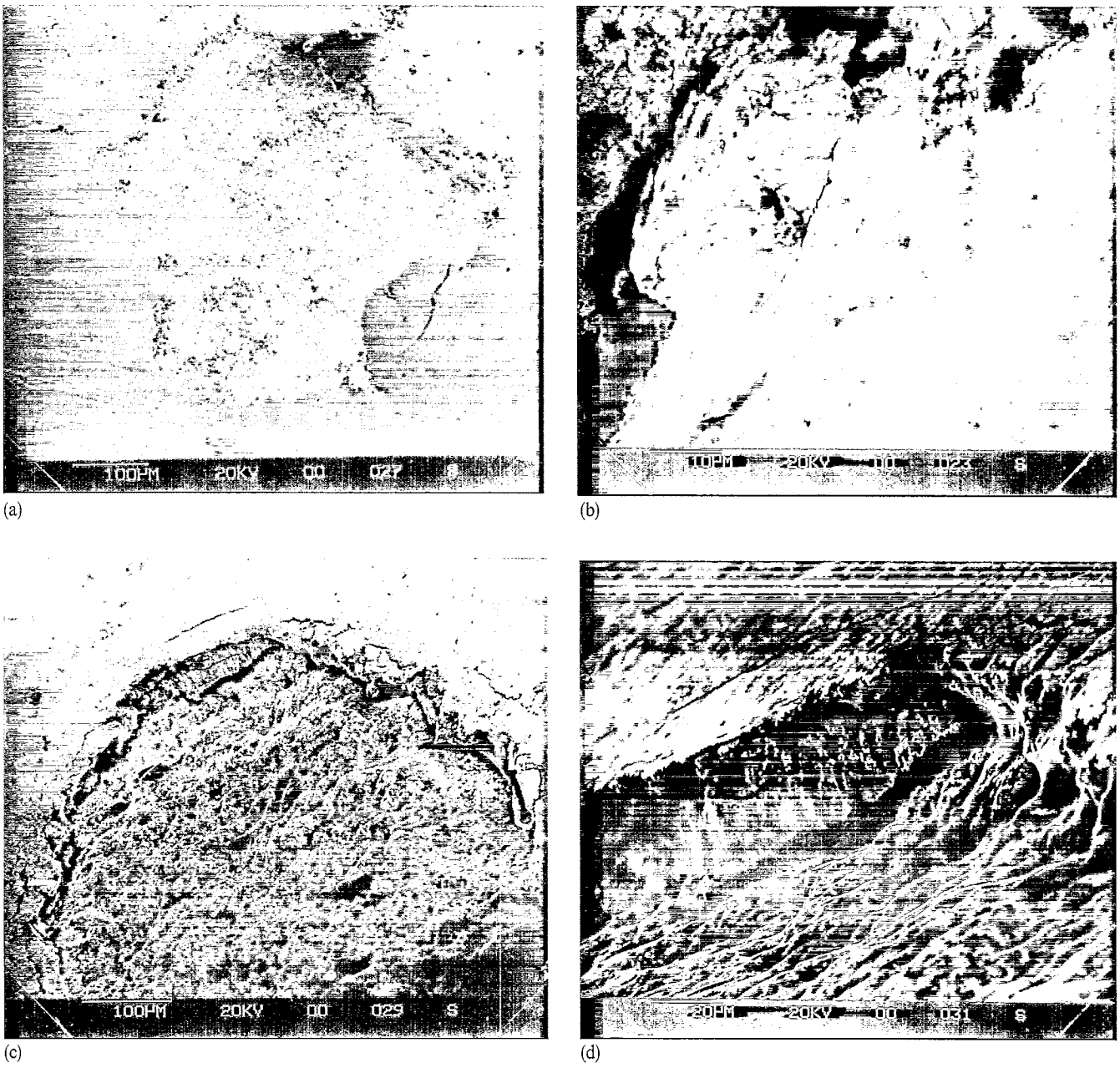

(a) (b) (c) (d)

Fig. 8. Observations of tungsten carbide coating–ceramic contact (Hitec 174 lubricant): (a) overview of failed area (160 N load); (b) edge crack detail; (c) failed area (400 N load); (d) cliff edge (crack propagation).

5. Discussion

The microstructure of thermal spray coatings is largely dependent upon the spraying method and the parameters during spraying, e.g. particle size, type of powder used, velocity of spray, surrounding atmosphere and substrate temperature. The porosity and secondary phase particles in the coating normally lead to stress concentrations. It is a well-established fact that the brittleness and weakness of sprayed coatings are due to their lamellar structure, where individual lamellae do not adhere to one another completely. Hence the use of these coatings is limited to low stress applications. A cryogenic fracture study of plasma-sprayed WC coatings by George and Vander Voort [11] revealed that these coatings not only have significant porosity but also secondary phase particles and lack of fusion. The delamination failure of these coatings can be thought of as a result of three effects, i.e. lamellar structure, porosity and secondary phase particles.

A study of ceramic coatings by Tobe et al. [3] and Hadfield et al. [5] indicates that the failure mechanism of ceramic coatings is different from that of WC–Co coatings. In the case of ceramic coatings the adhesive strength seems to be lower than the cohesive strength of the bulk coating and it represents a mismatch between substrate and coating materials.

It can be seen from SEM results that regardless of

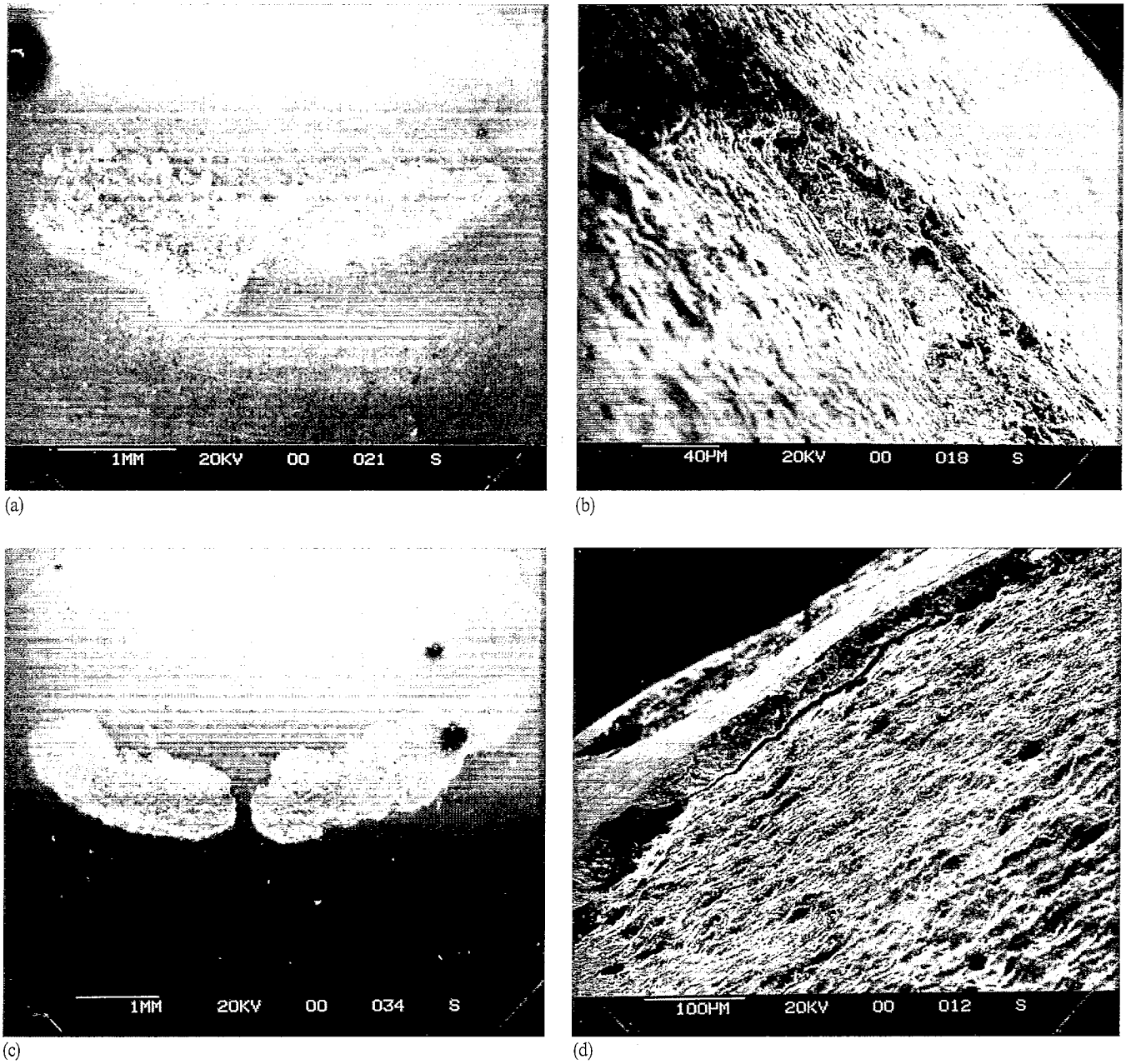

(a) (b) (c) (d)

Fig. 9. Observations of tungsten carbide coating–steel contact (160 N load): (a) failed area (Hitec 174 lubricant); (b) detail of failed area; (c) failed area (Exxon 2389 lubricant); (d) cliff edge.

changes in load, lubricant and contact configuration the failure mode remains as delamination at a depth of approximately 40 μm. The existence of edge cracks on the failed surfaces indicates that the coating failure is related to tensile stresses. FEM results reveal that although maximum principal shear, von Mises and Tresca stresses exist at the interface, the maximum shear stress in the X–Y plane is located at the depth of failure. A stress concentration in the coating followed by the rolling motion of the ball causes abrupt changes in stress at this depth. Although the magnitude of stress at this location is less than that of stresses occurring at the interface, the stress range is maximum at this depth because of the rolling motion. Owing to non-homogeneity and the presence of porosity, etc. in the coating microstructure, the coating cannot cope with these abrupt changes in stress and consequently delaminates. The fact that the coating does not fail at the interface means that there is sufficient adhesive bonding between the coating and the substrate. Moreover, the mechanical interlocking due to sandblasting of the substrate prior to coating improves coating adhesion and prevents coating failure at the interface.

FEM results indicate that changes in coating thickness will have very little effect on the dominant stresses. Thus an improvement in material properties of the coating such as porosity, homogeneity, Young modulus, Poisson ratio and toughness can be helpful in improving the

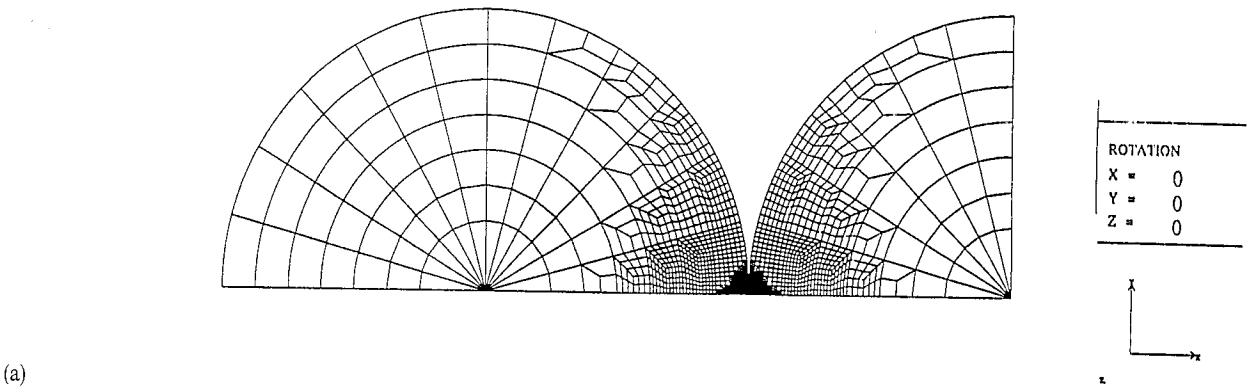

(a)

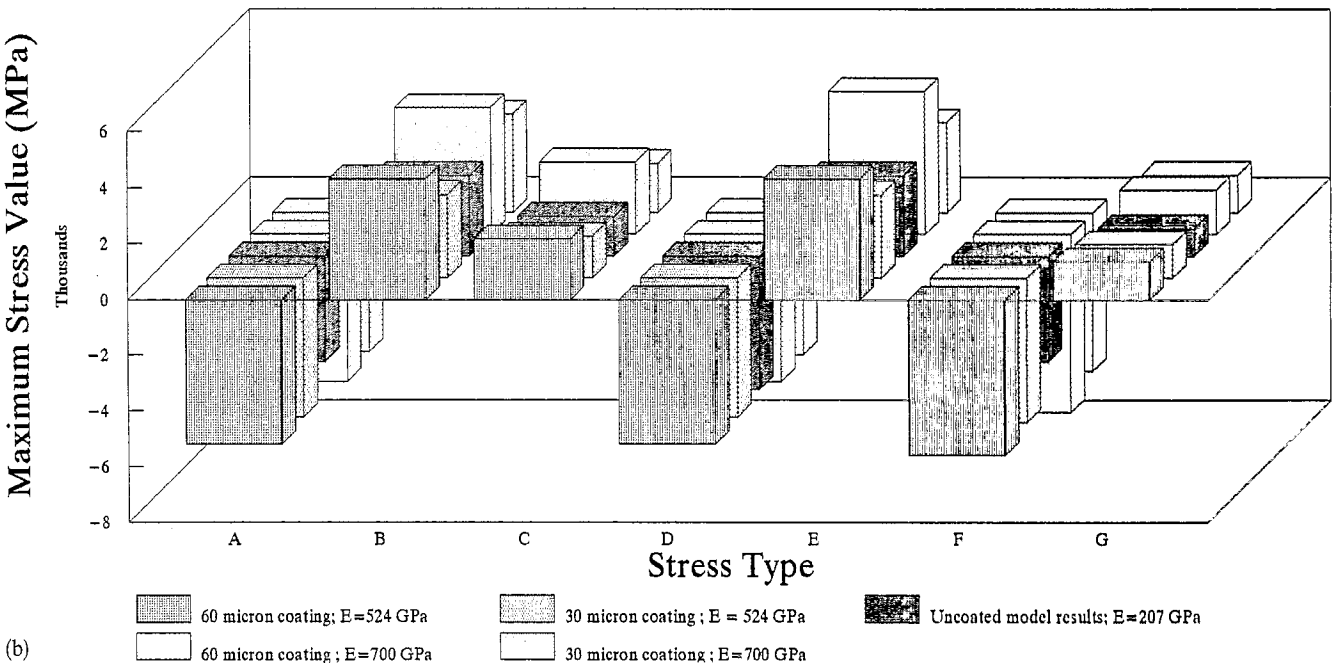

(b)

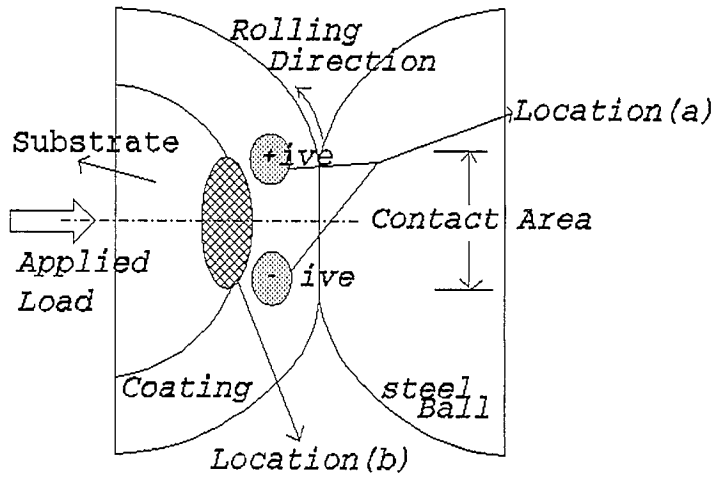

(c)

Fig. 10. (a) Axisymmetric finite element model of contacting balls. (b) Summary of FEM results: A, maximum principal stress; B, Tresca stress; C, maximum principal shear stress; D, maximum compressive stress; E, von Mises stress; F, hoop stress; G, shear stress in X–Y plane. (c) Location of stresses in coated element: location (a), maximum shear stresses in X–Y and Y–Z planes; location (b), maximum principal shear, von Mises and Tresca stresses.

performance. An observation from FEM analysis is that a change in coating thickness influences the location of dominant stresses but their magnitude does not change significantly.

The results of microhardness tests on the substrate indicate that the substrate hardness is low. Microhardness tests on standard rolling element bearing balls indicate an average hardness of 850 HV. This value is

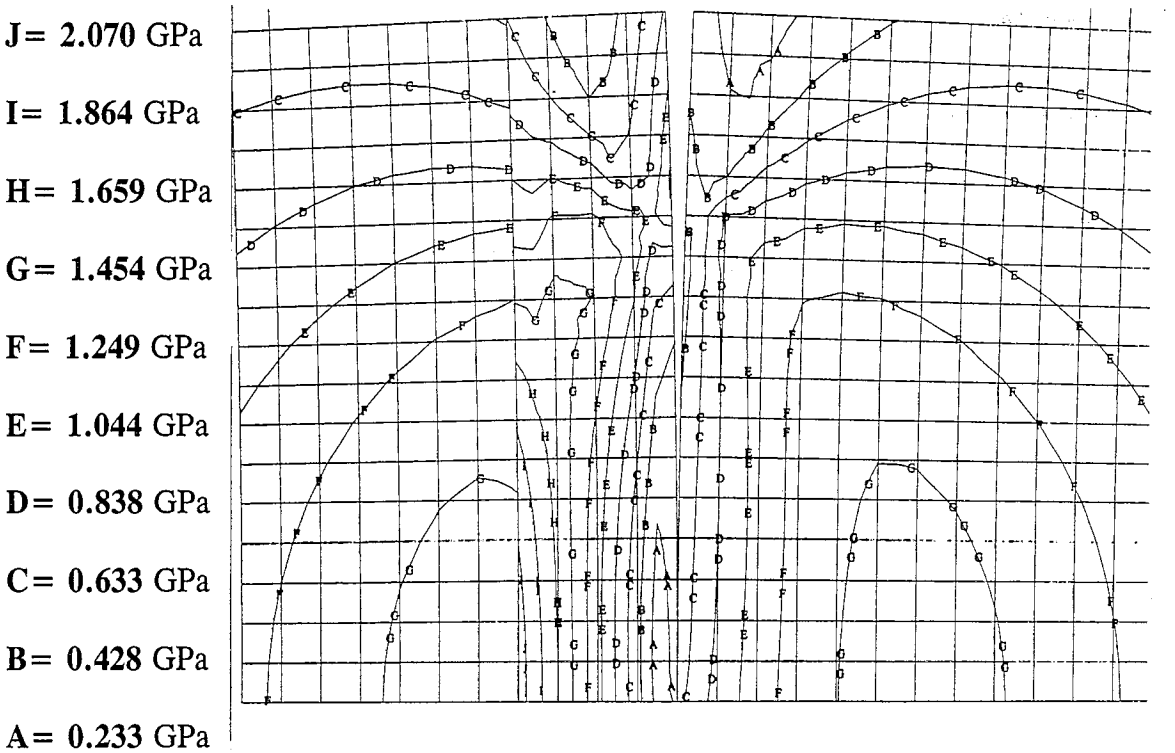

(a)

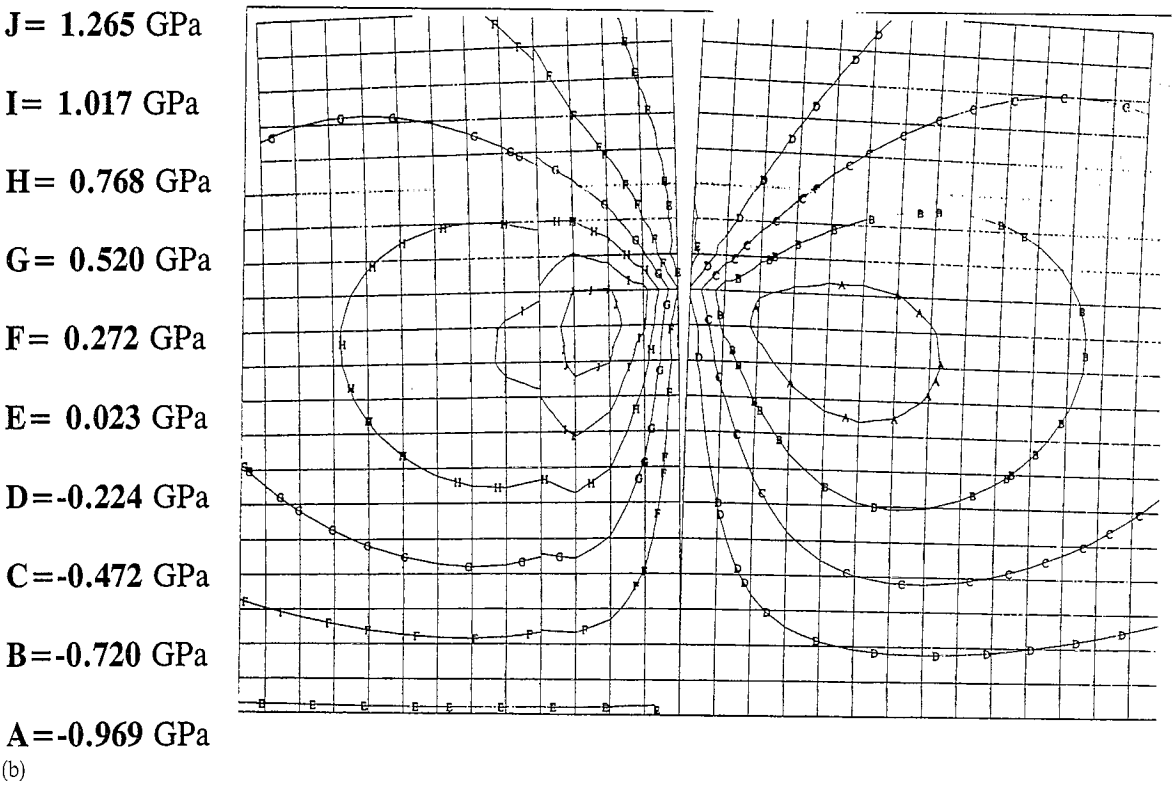

(b)

Fig. 11. (a) Maximum principal shear stress distribution. (b) Shear stress distribution in X–Y plane.

41% higher than the substrate hardness value of 600 HV. Microhardness measurements showed a variation in Vickers hardness throughout the coating section. This is in accordance with the analysis presented by Lin and Berndt [12]. A solution could be to use either the HIP method or heat treatment, although other coating methods such as HVOF and HVAF might also be investigated.

6. Concluding remarks

Edge cracks may have initiated fatigue failure on the surfaces of coatings. Delamination occurred through the coating itself.

Microhardness measurements revealed that the coating microhardness varies through its section. Moreover, the microhardness of the coating is twice that of the substrate.

Finite element modelling revealed that the effect of changing the coating thickness is to alter the location of stresses more abruptly than their magnitude.

Acknowledgements

The authors would like to thank Professor Shogo Tobe of Ashikaga Institute of Technology, Japan for his help in the preparation of coatings. The authors also acknowledge the financial support by the Overseas Research Scholarship Scheme which is partly funding this research project.

References

[1] A. Ohmori, Thermal spraying, current status and future trends, *Proc. Int. Thermal Spray Conf., Kobe, May 1995*, High Temperature Society of Japan, Kobe, 1995.

[2] P. Vuoristo, K. Niemi, A. Makela and T. Mantyla. Spray parameter effects on structure and wear properties of detonation gun sprayed WC–17%Co coatings, *Proc. Nat. Thermal Spray Conf. Anaheim, CA, 1993*, ASM International, Anaheim, CA, 1993, pp. 173–178.

[3] S. Tobe, S. Kodama and H. Misawa. Rolling fatigue behaviour of plasma sprayed coatings on aluminium alloy, *Proc. Nat. Thermal Spray Conf., Tokyo, Japan, 1990*, ASM International, Anaheim, CA, pp. 171–178.

[4] M.K. Keshavan and K.T. Kembaiyan. Wear characterization and practical applications of thermal spray coatings in drilling applications, *Proc. Natl. Thermal Spray Conf., Anaheim, CA, 1993*, ASM International, Anaheim, CA, 1993, pp. 635–641.

[5] M. Hadfield, R. Ahmed and S. Tobe, Rolling contact fatigue of thermally spray coated cones, *Proc. Int. Thermal Spray Conf., Kobe, May 1995*, High Temperature Society of Japan, Kobe, 1995, pp. 1097–1102.

[6] R. Thom, L. Moore, W.D. Sproul and T.P. Chang, Rolling contact fatigue tests of reactively sputtered nitride coatings of Ti, Zr, Hf, Cr, Mo, Ti–Al, Ti–Zr, and Ti–Al–V on 440C steel, *Surf. Coat. Technol., 62* (1993) 423–427.

[7] W.D. Sproul, M.E. Graham, M. Wong and P.J. Rudnik, Reactive unbalanced magnetron sputtering of the nitride coatings of Ti, Zr, Hf, Cr, Mo, Ti–Al, Ti–Zr, and Ti–Al–V on 440C steel, *Surf. Coat. Technol., 61* (1993) 139–143.

[8] R. Tourret and E.P. Wright, Rolling contact fatigue: performance testing of lubricants, *Proc. Int. Symp., Institute of Petroleum, October 1976*, Heyden, London, 1977.

[9] K. Wira, C.W. Lin and N.L. Loh, Micro-structure and wear properties of arc sprayed tungsten carbide coatings, *Proc. Int. Thermal Spray Conf., Kobe, May 1995*, High Temperature Society of Japan, pp. 465–470.

[10] B.O. Jacobson, *Rheology and Elastohydrodynamic Lubrication*, Baker & Taylor, 1991.

[11] F. Vander Voort, A layman's view of plasma spray coating metallography, *Structure 28*, (1995) 8–13.

[12] C.K. Lin and C.C. Berndt, Micro-hardness variations in thermally sprayed coatings, *Proc. Natl. Thermal Spray Conf., Anaheim, CA, 1993*, ASM International, Anaheim, CA, 1993, pp. 561–568.